COBEM 2023 27TH INTERNATIONAL CONGRESS OF MECHANICAL ENGENEERING

ABCM Brazilian Society of Mechanical Sciences and Engineering
27th ABCM International Congress of Mechanical Engineering
December 04-08, 2023, Florianópolis-SC, Brazil

COB-2023-1700
DESIGN AND ANALYSIS OF A TOPOLOGICAL PIEZOELECTRIC METAMATERIAL BEAM

Luis Alfredo Pérez Martínez
Department of Aeronautical Engineering, Sao Carlos School of Engineering, University of Sao Paulo, Brazil
luisperezm@usp.br

Danilo Beli
Department of Mechanical Engineering, Eindhoven University Of Technology, The Netherlands
beli.danilo@gmail.com

Carlos De Marqui Jr
Department of Aeronautical Engineering, Sao Carlos School of Engineering, University of Sao Paulo, Brazil
demarqui@sc.usp.br

Abstract. *Topological metamaterials present novel properties and phenomena, including topological interface states, energy localization, and robust localization. Topological interface states have been mostly reported in the literature in systems whose polarization transition is due to phononic crystal features of the host structure (Bragg scattering). This paper shows that polarization transition and interface states can be observed in piezoelectric metamaterial beams with interconnected resonant shunt circuits. An electromechanically coupled finite element model is presented. The band structure presents a resonant bandgap and two folding points for a certain unit cell configuration with uncoupled resonant shunt circuits. The conditions for opening bandgaps at the folding points, band inversion, and polarization transition are discussed. The proposed topological metamaterial comprises two media with different circuit interconnection parameters. Topological interface states are evidenced in the band structure and vibration energy localization observed in the forced response.*

Keywords: *Piezoelectricity, Topological metamaterial, Polarization transition, Interface state*

1. INTRODUCTION

Topological insulator materials (TIs) have attracted considerable interest in recent years. TIs were originally studied and explored in the condensed matter physics area (Hasan and Kane (2010)) and later extended to phononic crystals (Yang *et al.* (2015),Yin *et al.* (2018)) and elastic metamaterials (Pal and Ruzzene (2017)), paving the way to obtain waveguides without backscattering and immune to defects. Band inversion and polarization transition are considered indications that topological interface states can occur. The presence of interface modes can be predicted calculating topological invariants, such as the Zak phase (Zak (1989)), which can be used to characterize the topological properties of bands. In addition to the direct calculation, the Zak phase of an isolated band can be estimated by analyzing the symmetry and anti-symmetry of its band-edge states (Zhu *et al.* (2018)).

Strategies such as modification of the geometric topology and constitutive parameters to break the mirror symmetry of a unit cell have been widely used as an effective means to achieve mode polarization transition. (Zhao *et al.* (2018)) designed a locally resonant acoustic system to produce three band gaps in the subwavelength region; one originated from the local resonance, and the other two from the Bragg-scattering. The authors concluded that interface states can only exist in Bragg-scattering band gaps. Through the band-folding technique, (Liu *et al.* (2021)) also realized two topological interface states in a beam with periodically arranged elastic local resonators. The substructure is also covered with piezoelectric layers shunted with negative capacitance circuits. They show band inversion and polarization transition with negative capacitance parameter variation. Designs developed in the above-mentioned studies rely on a host structure with a phononic crystal feature to achieve polarization transition. (Hu *et al.* (2022)) presented a locally resonant metamaterial without any phononic crystal feature, where the band inversion and polarization transition are achieved by manipulating the design of local resonators.

This paper presents a topological piezoelectric metamaterial inspired by the system proposed by (Hu *et al.* (2022)). The occurrence of topologically protected interface modes (TPIMs) is investigated by presenting the band structure, polarization transition, and the forced response of the electromechanically coupled metamaterial. The results show that by adjusting electrical parameters, multiple interface states can be observed.

2. ELECTROMECHANICAL TOPOLOGICAL METAMATERIAL MODEL

Consider an elastic beam bracketed by two piezoelectric layers poled in the same direction. Each piezoelectric layer is covered on top and bottom surfaces by thin layers of conductive electrodes that are periodically segmented. Each segmented electrode is connected in parallel to an inductive shunt circuit to induce local resonance in the structure. The boundaries of each segmented electrode region delimit the fundamental unit cell. The right boundary of the *j*th fundamental unit cell and the left boundary of the (*j*+1) fundamental unit cell share the same mechanical degrees of freedom (DOFs). To investigate the topological properties, a new unit cell that comprises a pair of fundamental unit cells interconnected with a capacitor is defined in Fig. 1. The electromechanically coupled unit cell defined in Fig. 1 is analogous to the elastic one studied in (Hu *et al.* (2022)).

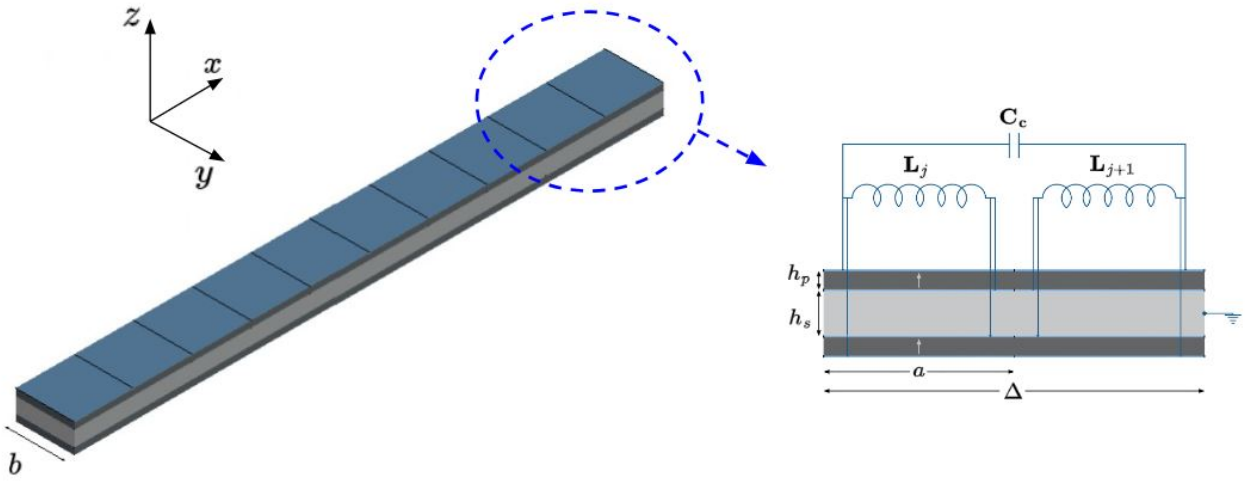

Figure 1: Piezoelectric metamaterial beam with segmented electrodes in a bimorph configuration (left) and its unit cell in detail (right). The colored regions correspond to the substructure (gray), piezoelectric metamaterial (dark gray), the electrodes (blue), and the shunt circuit associated with the system (dark blue).

Euler-Bernoulli assumptions are considered in formulating an electromechanically coupled finite element (FE) model of the metamaterial beam. The structure is discretized into one-dimensional beam elements (Petyt (2010)). Each element has two nodes, each with two degrees-of-freedom (DOF) and defined as the transverse displacement (w) and the rotation θ about the y direction. In the model derivation, the effect of the structural damping is not considered. Thus, the dynamic behavior of the electromechanical metamaterial beam is described by the set of global equations of motion (De Marqui Junior *et al.* (2009))

$$\mathbf{M\ddot{u}} + \mathbf{Ku} - \mathbf{\Theta v} = \mathbf{F}, \tag{1a}$$

$$\mathbf{C_p v} + \mathbf{q} + \mathbf{\Theta^t u} = \mathbf{0}, \tag{1b}$$

where $\mathbf{M}$ is the global mass matrix $(m \times m)$, $\mathbf{K}$ is the global stiffness matrix $(m \times m)$, $\mathbf{\Theta}$ is the electromechanical coupling matrix $(m \times e)$, $\mathbf{C_p}$ is the capacitance matrix $(e \times e)$, $\mathbf{F}$ is the vector of mechanical forces $(m \times 1)$, $\mathbf{v}$ is the vector of the voltage output from pairs of segmented electrodes $(e \times 1)$, $\mathbf{q}$ is the vector of electrical charges $(e \times 1)$, and $\mathbf{u}$ is the vector of mechanical DOFs $(m \times 1)$, which contains the trasverse displacement (u) and rotations (θ) associated to each node. In addition, m and e refer to the number of mechanical and electrical DOFs respectively. The over-dots denote time derivation, and t is the matrix transpose when used as a superscript. Each unit cell is connected to inductances and then Eq. (1a) and (1b) can be written in matrix form as,

$$\begin{bmatrix} \mathbf{M} & \mathbf{0} \\ \mathbf{\Theta^t} & \mathbf{C_p} \end{bmatrix} \begin{bmatrix} \ddot{\mathbf{u}} \\ \ddot{\mathbf{v}} \end{bmatrix} + \begin{bmatrix} \mathbf{K} & -\mathbf{\Theta} \\ \mathbf{0} & \mathbf{L}^{-1} \end{bmatrix} \begin{bmatrix} \mathbf{u} \\ \mathbf{v} \end{bmatrix} = \begin{bmatrix} \mathbf{F} \\ \mathbf{0} \end{bmatrix}, \tag{2}$$

with mechanical and electrical domains coupled by the off-diagonal terms, where $\mathbf{L}$ is a $(e \times e)$ diagonal matrix that contains the inductances of each shunt circuit. They can be tuned to an electrical resonance at a selected frequency $(\omega_\mathbf{r})$ (Hagood and Flotow (1991)),

$$\omega_{\mathbf{r}} = \mathbf{1}/\sqrt{\mathbf{C}_{\mathbf{p}_j}\mathbf{L}_j} \tag{3}$$

where $\mathbf{C}_{\mathbf{p}_j}$ and $\mathbf{L}_j$ are de capacitance of the *j*th of fundamental unit cell and the inductance of the *j*th shunt circuit.

Table 1: Material properties for the aluminum substructure and the PMN-PT

Property	Value
Young's modulus of the substructure	69 GPa
Mass density of the substructure	2700 Kg/m^3
Mass density of the piezoelectric material	8120 Kg/m^3
Elastic compliance at constant electric field, s_{11}^E	45.9×10^{-12}
Piezoelectric strain coefficient, d_{31}	-646×10^{-12} V/m
Piezoelectric permittivity constant at constant stress, ε_{33}^T	4.208×10^{-8} F/m

The subscript numbers refer to the Voigt notation of the s, d and ε tensors, where 1, 2 and 3 corresponds to the x, y and z directions, respectively (De Marqui Junior *et al.* (2009))

3. BAND INVERSION AND POLARIZATION TRANSITION

Since a piezoelectric element can be represented as a current source in parallel with its internal capacitance (Ottman *et al.* (2002)), the electrical representation of the electroelasic unit cell presented in Fig. 1 is represented by the electric circuit shown in Fig. 2. Applying the Kirchoff law, one can obtain,

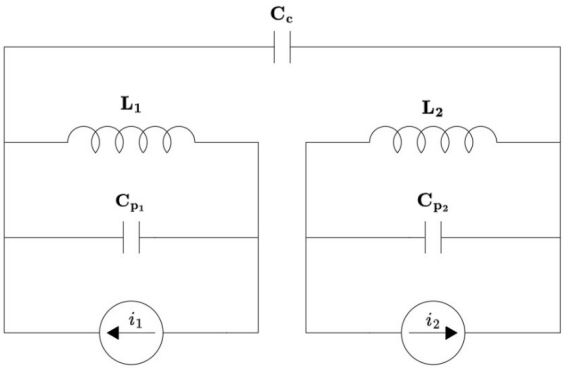

Figure 2: Topological unit cell represented as an electric circuit

$$i_{\mathbf{1}} = \mathbf{C}_{\mathbf{p_1}}\dot{\mathbf{v}}_{\mathbf{1}} + \mathbf{C}_{\mathbf{c}}(\dot{\mathbf{v}}_{\mathbf{1}} - \dot{\mathbf{v}}_{\mathbf{2}}) + \frac{\xi_{\mathbf{1}}}{\mathbf{L_1}}, \tag{4a}$$

$$i_{\mathbf{2}} = \mathbf{C}_{\mathbf{p_2}}\dot{\mathbf{v}}_{\mathbf{2}} + \mathbf{C}_{\mathbf{c}}(\dot{\mathbf{v}}_{\mathbf{2}} - \dot{\mathbf{v}}_{\mathbf{1}}) + \frac{\xi_{\mathbf{2}}}{\mathbf{L_2}}, \tag{4b}$$

where ξ is an auxiliary variable with $\dot{\xi}_j = \mathbf{v}_j$, and $\mathbf{C_c}$ is the capacitance of the coupling capacitor defined in this work as,

$$\mathbf{C_c} = \delta \mathbf{C}_{\mathbf{p}_j}, \tag{5}$$

and δ is a dimensionless parameter defined as the coupling capacitance to the effective piezoelectric capacitance of the fundamental unit cell ratio. Note that based on Eq. 4, the elements in the diagonal of the new capacitance matrix are the sum of $\mathbf{C}_{\mathbf{p}_j}$ and $\mathbf{C_c}$, the off-diagonal terms represent the internal coupling of the unit cell.

For the following results, we consider a unit cell with dimensions $a = 1 \times 10^{-3}$ m, $b = 12.7 \times 10^{-3}$ m, $h_p = 0.25 \times 10^{-3}$ m, and $h_s = 0.167 \times 10^{-3}$ m. The aluminum substructure is bracketed by two piezoelectric layers of PMN-PT poled in the z direction with properties presented in Table 1. The resulting electrodes are connected in parallel to an inductive shunt circuit syntonized to induce electrical resonance at the frequency $\omega_r = 2000$ Hz.

3.1 Band inversion

The dispersion calculation is performed by applying the Bloch-Floquet conditions at the boundaries of the unit cell and then solving a quadratic eigenvalue problem through all values of the wavenumber along the first irreducible Brillouin (Orms and Petyt (1974); Thomes *et al.* (2022)).

The band structure of the unit cell defined in Fig. 1 is displayed in Fig.3b for $\delta = 0$. In such a case, the metamaterial becomes a periodic locally resonant metamaterial. It is noted that there is only a single locally resonant band gap (LRBG). Folding points, regarded as band-transition points, appear above and below the LRBG. Fig.3a and c shows that when $\delta \neq 0$ the transition points open in two new band gaps.

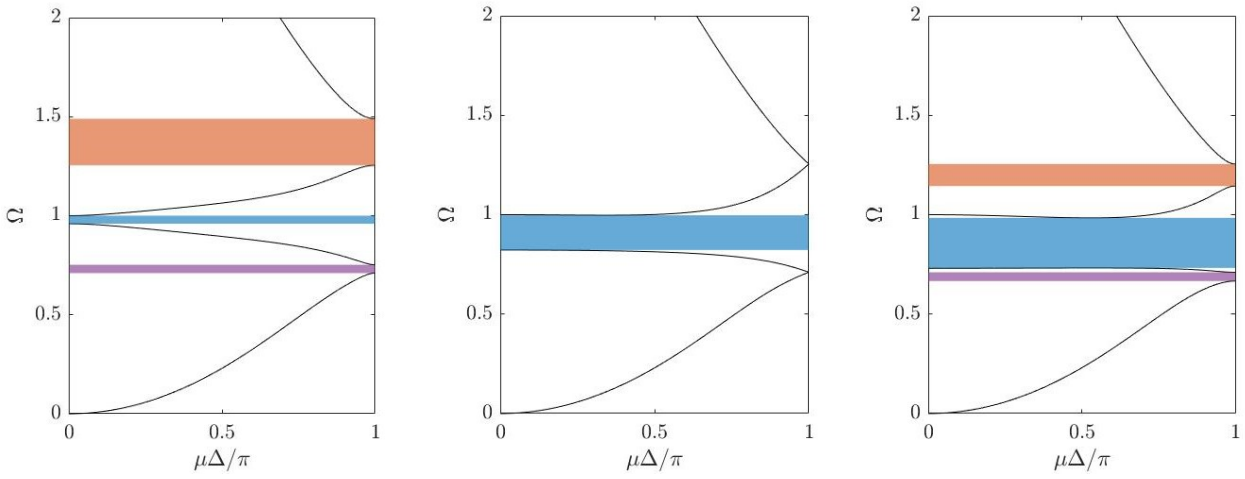

Figure 3: Bands structures of the internally coupled metamaterial with different dimensionless coupling parameters: (a) $\delta = -0.2$, (b) $\delta = 0$, (c) $\delta = 0.2$. The color-shaded areas represent the band gaps. μ is the wavenumber, and Ω is the normalized frequency ω/ω_r.

Figure 4 shows the band evolution. The curves I∼IV are associated with the maximum and minimum eigenvalues at the six bounds of the band gaps. Each eigenvalue has a corresponding eigenvector that contains modal information of the dynamic system. Therefore, each curve in Fig, 4 is associated with a mode.

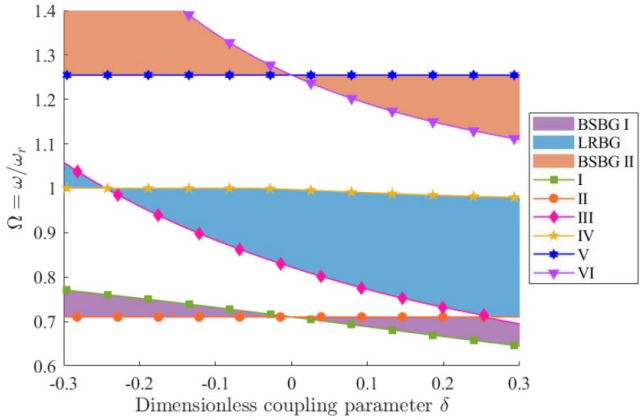

Figure 4: Band gap evolution for varying δ. Curves I $\sim$ VI represent a mode shape associated with the band gap limits.

The three points where a band gap closes and reopens are transition points in Fig. 4. The transition points at $\delta = 0$ are related to band gaps BSBG I and II. For the LRBG the transition point is observed for $\delta_r \approx -0.245$.

3.2 Polarization transition

As mentioned above, each curve in Fig. 4 refers to a specific mode shape. When polarization transition occurs, the topology properties of the unit cell change. Note that the evolution for each band gap at the left and right of a transition point is supposed to be opposite processes. Therefore, band inversion is a necessary condition for polarization transition.

Figure 5 displays the normalized mode shapes associated with curves I∼VI. Note that for curves I, II, V, and VI,

polarization transition occurs at $\delta = 0$, and for curves III and IV at $\delta = \delta_r$. Therefore, it is evident that the mode shapes are switched just after their respective transition point, which means that the mode evolution on either side of a transition point is an opposite process. Topological interface states can be observed at the interface of two unit cells with different topological properties (Hu *et al.* (2022)).

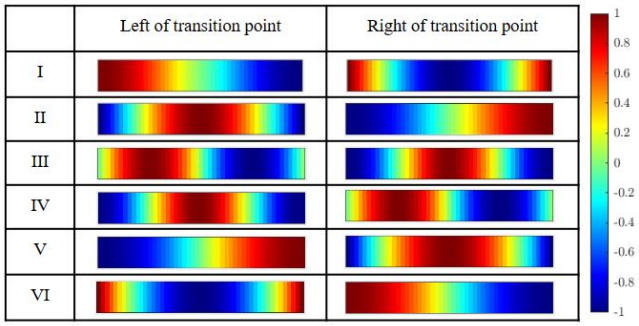

Figure 5: Unit cell mode shape associated with curves I∼VI for the left and right side of its respective transition points

4. INTERFACE STATES

In the previous sections, criteria such as band inversion and polarization transition were used to predict the existence of topological interface modes (TPIMs) in the piezoelectric metamaterial beam. A topological metamaterial beam is considered in the present section, which satisfies the previously defined conditions to demonstrate the existence of TPIMs through the forced response.

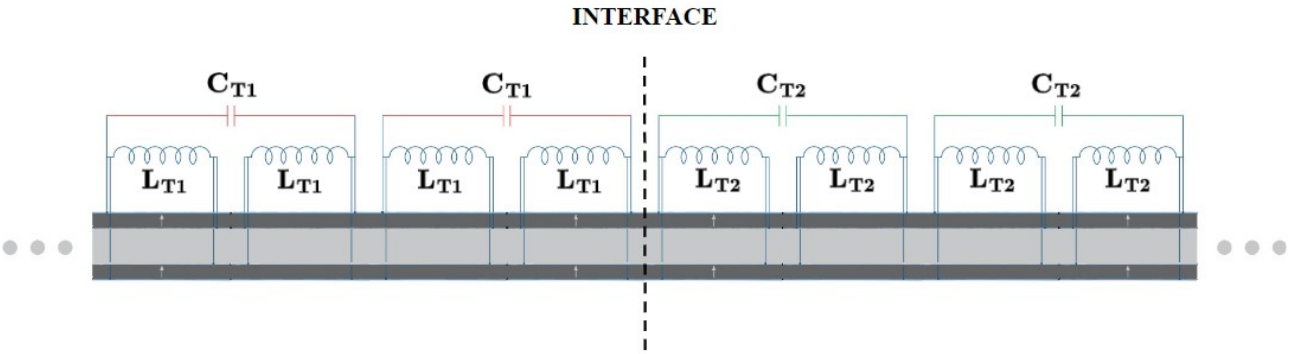

Figure 6: A locally resonant metamaterial piezoelectric metamaterial beam which is assembled by two types of topologies ($\mathbf{T1}$ and $\mathbf{T2}$) on the left and right side, respectively.

Consider the structure shown in Fig. 6, with $2N$ unit cells (N unit cells at each interface side). Each media (left and right) has unit cells with distinct topologic properties (regarded as $\mathbf{T1}$ for the left-hand side and $\mathbf{T2}$ for the right-hand side), as discussed in the previous section. Note in Fig. 4 that each band gap is non-symmetrical regarding its respective transition point; thus, it is necessary to tune the circuit parameters ($\mathbf{L}$ and $\mathbf{C_c}$) to match the band gaps of the right and left media. Fig.(4) shows that the width of the band gaps is related to δ. On the other hand, ω_r changes the frequency at which the band transition points emerge and, consequently, the range of frequencies where non-trivial band gaps open. Therefore, by adjusting these two parameters, one can adjust the range of frequencies and width of the band gaps. In this work, parameters $\mathbf{C_{T1}}$ and $\mathbf{L_{T1}}$ for $\delta_{\mathbf{T1}} = 0.23$ and resonance frequency $\omega_{\mathbf{T1}} = 2000$ Hz are fixed. Then, $\mathbf{C_{T2}}$ and $\mathbf{L_{T2}}$ are determined by employing a searching algorithm to match the selected band gaps.

The forced response is computed by assuming harmonic excitation $\mathbf{F}(t) = \bar{\mathbf{F}}(\omega)e^{\mathbf{i}\omega t}$ in Eq. 2 and, consequently, $\mathbf{u}(t) = \mathbf{u}(\omega)e^{\mathbf{i}\omega t}$, $\mathbf{v}(t) = \mathbf{v}(\omega)e^{\mathbf{i}\omega t}$, where ω is the angular frequency and $\mathbf{i}$ is the imaginary unit number. The harmonic punctual excitation is applied at the middle of the structure (interface at $L/2$, where L the total length of the topological metastructure), and the amplitude of transverse displacement $\bar{w}(x, \Omega)$ is computed.

Figures 8, 10, and 12 displays the harmonic response, $20\log_{10}|\bar{w}(x,\Omega)/\bar{F}(L/2,\Omega)|$ (dB, reference 1m/N) along the structure. The distribution of the topologies on the structure is defined as follows: $\mathbf{T1}$ for values from $x = 0$ to $x = 0.5L$, and $\mathbf{T2}$ from $x = 0.5L$ to $x = L$, where $x = 0.5$ is the interface point. Figures 7b, 9b, and 11b depict the harmonic response at $x = 0$ and $x = L$.

4.1 Topological interface state in the BSBG I

To demonstrate the interface state formation in the first band gap we considered $N = 15$ and the left-hand topology ($\mathbf{T1}$) with fixed parameters $\delta_{\mathbf{T1}} = 0.23$ and $\omega_{\mathbf{T1}} = 2000$ Hz. Then, the parameters of the right-hand topology ($\mathbf{T2}$) are determined as: $\delta_{\mathbf{T2}} = -0.1981$ and $\omega_{\mathbf{T2}} = 1786$ Hz. Fig. 7a shows that the band gaps due to $\mathbf{T1}$ and $\mathbf{T2}$ overlap for the BSBG I. Figure 7b exhibits the harmonic response at each end of the structure (solid dark line for $x = 0$ and dashed blue line for $x = L$) for a frequency range containing BSBG I. The continuous red lines defines the band gap frequency limits.

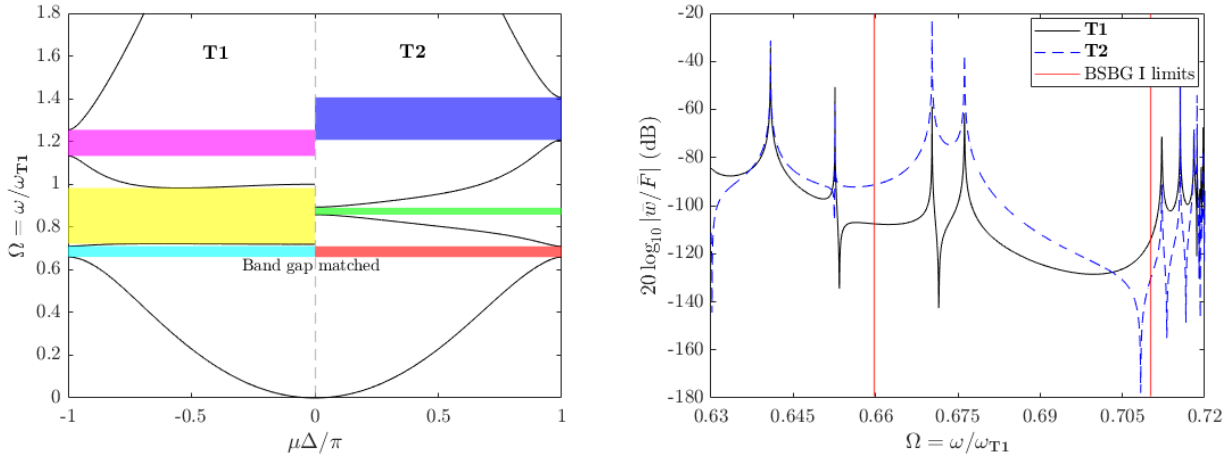

(a) (b)

Figure 7: (a) Comparison of the band structures of the two topologies present in the heterostructure, with $\delta_{\mathbf{T1}} = 0.23$, $\omega_{\mathbf{T1}} = 2000$ Hz, $\delta_{\mathbf{T2}} = -0.1981$, and $\omega_{\mathbf{T2}} = 1786$ Hz. The color-shaded areas denote the band gaps. (b) Harmonic response for $\mathbf{T1}$ and $\mathbf{T2}$ at $x = 0$ and $x = L$, respectively.

Note in Fig. 7b that two peaks arise within the band gap zone. A peak is at $\Omega = 0.676$, which is regarded as an interface mode, and the other at $\Omega = 0.670$ which is an edge mode, that will not be discussed in the present work. Figure 8 displays a harmonic response map as a function of the space and frequency. For $\Omega = 0.676$, vibration energy is localized around the interface.

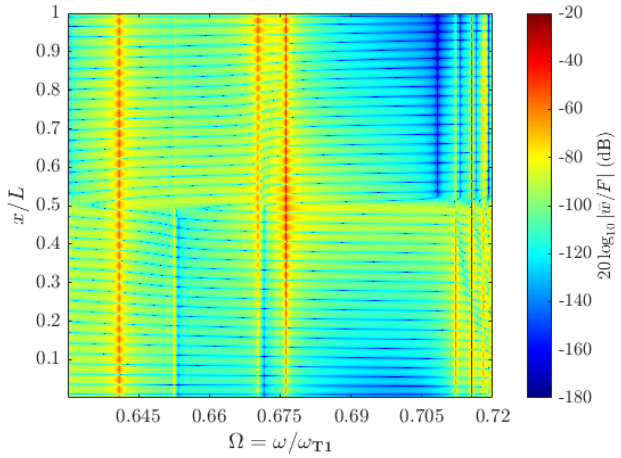

Figure 8: Harmonic response map as a function of the space and frequency values containing BSBG I.

4.2 Topological interface state in the LRBG

We now proceed to obtain TPIM in the LRBG. Note that the transition point is located at $\delta = \delta_r$ for this case. Therefore, it is a necessary condition that $\delta_{\mathbf{T1}} > \delta_r$ and $\delta_{\mathbf{T2}} < \delta_r$ or vice-versa. Considering $N = 15$, $\delta_{\mathbf{T1}} = -0.20$ and $\omega_{\mathbf{T1}} = 2000$ Hz, the parameters of $\mathbf{T2}$ are determined as $\delta_{\mathbf{T2}} = -0.284$ and $\omega_{\mathbf{T2}} = 1915.7$ Hz. Figure 9a shows that the band gaps due to $\mathbf{T1}$ and $\mathbf{T2}$ share the same frequency range for the LRBG. The harmonic response is plotted for $\mathbf{T1}$ and $\mathbf{T2}$ in Fig 9b. A sharp peak at $\Omega = 0.977$ corresponds to the TPIM inside an attenuation region induced by the local resonances of the structure. Figure 10 shows localization effect around the interface at $\Omega = 0.977$.

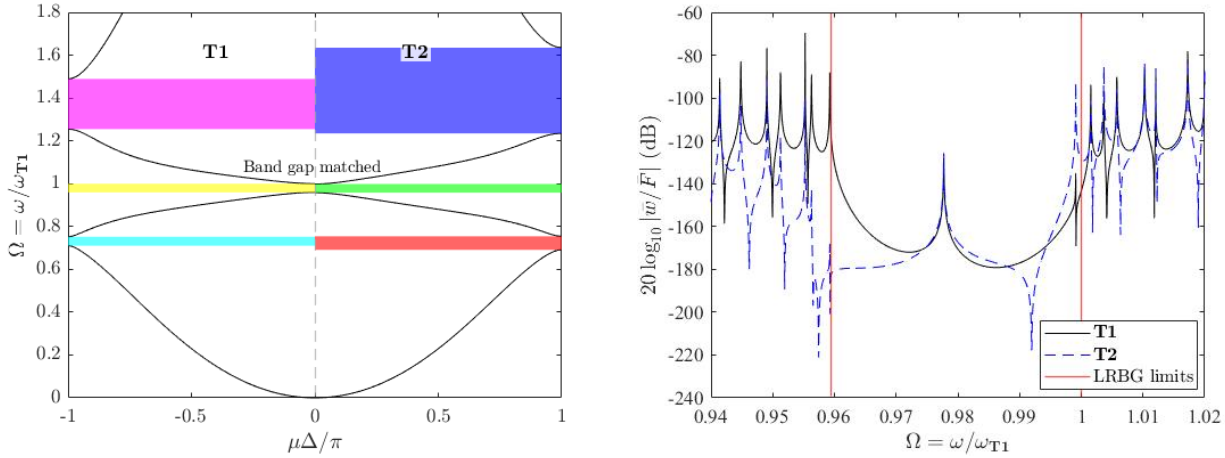

(a) (b)

Figure 9: (a) Comparison of the band structures of the two topologies present in the heterostructure, with $\delta_{\mathbf{T1}} = -0.2$, $\omega_{\mathbf{T1}} = 2000$ Hz, $\delta_{\mathbf{T2}} = -0.284$, and $\omega_{\mathbf{T2}} = 1915.7$ Hz. The color-shaded areas denote the band gaps. (b) Harmonic response for $\mathbf{T1}$ and $\mathbf{T2}$ at $x = 0$ and $x = L$, respectively.

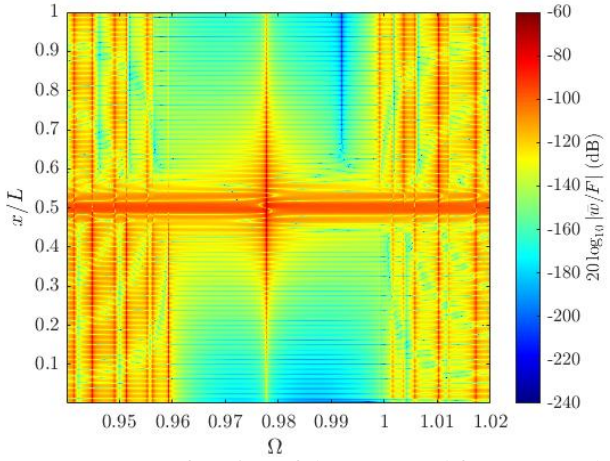

Figure 10: Harmonic response map as a function of the space and frequency values containing the LRBG.

4.3 Topological interface state in the BSBG II

To make evident the existence of the interface mode within BSBG II, it was necessary to increase the number of unit cells (N) for each topology. Considering $N = 40$, $\delta_{\mathbf{T1}} = 0.23$ and $\omega_{\mathbf{T1}} = 2000$ Hz, the parameters of $\mathbf{T2}$ are determined as $\delta_{\mathbf{T2}} = -0.1885$ and $\omega_{\mathbf{T2}} = 1269.5$ Hz. Figure 11a shows that the band gaps of $\mathbf{T1}$ and $\mathbf{T2}$ share the same frequency range for the BSBG II. As discussed in Fig. 7b, two peaks arise within the band gap zone in Fig. 11b. The interface interface mode is observed at the normalized frequency $\Omega = 1.2$. The vibration localization around the interface can be observed at the same frequency in Figure 12.

5. CONCLUSIONS

This work investigated a one-dimensional piezoelectric metamaterial beam with internally coupled electromechanical resonators to obtain three interface states in the sub-wavelength region. By modeling the electromechanically couple system with finite element model, the dispersion relation was computed, the band gap evolution investigated and mode shapes at the bounds of band gaps analyzed. Band inversion and polarization transition were discussed by analyzing band gap evolution and mode shapes.

A metamaterial composed of two media with different topologies was investigated. The coupling capacitance and resonance frequency were adjusted to achieve band gap overlaping. Vibration energy localization was observed at topologic interface states observed in three different band gaps.

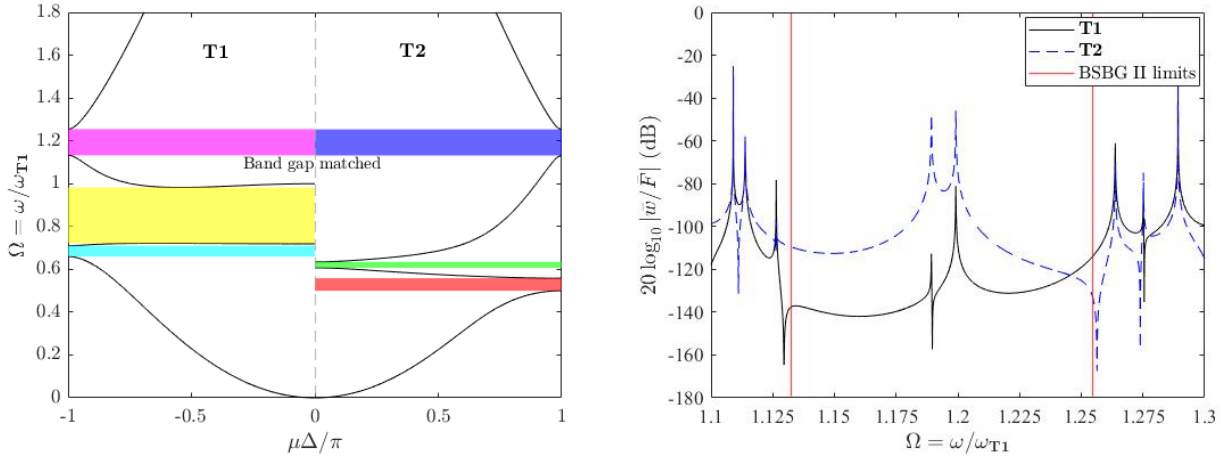

(a) (b)

Figure 11: (a) Comparison of the band structures of the two topologies present in the heterostructure, with $\delta_{\mathbf{T1}} = 0.23$, $\omega_{\mathbf{T1}} = 2000$ Hz, $\delta_{\mathbf{T2}} = -0.1885$, and $\omega_{\mathbf{T2}} = 1269.5$ Hz. The color-shaded areas denote the band gaps.

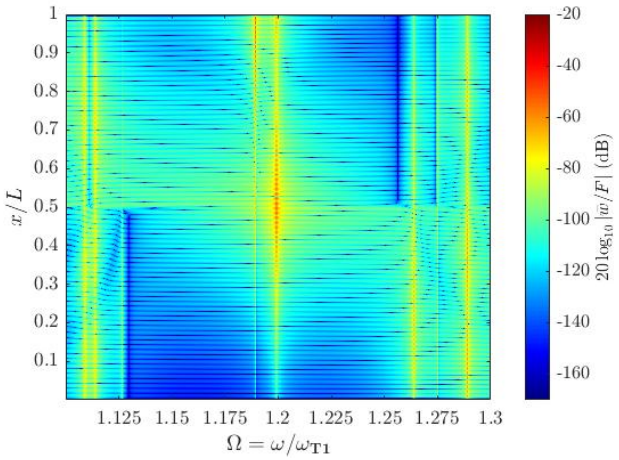

Figure 12: Harmonic response map as a function of the space and frequency values containing the LRBG.

6. REFERENCES

De Marqui Junior, C., Erturk, A. and Inman, D.J., 2009. "An electromechanical finite element model for piezoelectric energy harvester plates". *Journal of Sound and Vibration*, Vol. 327, No. 1, pp. 9–25. ISSN 0022-460X. doi:https://doi.org/10.1016/j.jsv.2009.05.015. URL `https://www.sciencedirect.com/science/article/pii/S0022460X09004520`.

Hagood, N.W. and Flotow, A.V., 1991. "Damping of structural vibrations with piezoelectric materials and passive electrical networks".

Hasan, M.Z. and Kane, C.L., 2010. "Colloquium: Topological insulators". *Rev. Mod. Phys.*, Vol. 82, pp. 3045–3067. doi:10.1103/RevModPhys.82.3045. URL `https://link.aps.org/doi/10.1103/RevModPhys.82.3045`.

Hu, G., Lan, C., Tang, L. and Yang, Y., 2022. "Local resonator stimulated polarization transition in metamaterials and the formation of topological interface states". *Mechanical Systems and Signal Processing*, Vol. 165. ISSN 10961216. doi:10.1016/j.ymssp.2021.108388.

Liu, Y., Wang, H., Fang, W., Han, Q., Liu, D. and Liang, Y., 2021. "Tunable control of subwavelength topological interface modes in locally resonance piezoelectric metamaterials". *Composite Structures*, Vol. 276. ISSN 02638223. doi:10.1016/j.compstruct.2021.114541.

Orms, R.M. and Petyt, M., 1974. "A finite element study of harmonic wave propagation in periodic structures".

Ottman, G., Hofmann, H., Bhatt, A. and Lesieutre, G., 2002. "Adaptive piezoelectric energy harvesting circuit for wireless remote power supply". *IEEE Transactions on Power Electronics*, Vol. 17, No. 5, pp. 669–676. doi:10.1109/TPEL.2002.802194.

Pal, R.K. and Ruzzene, M., 2017. "Edge waves in plates with resonators: An elastic analogue of the quantum valley hall

effect". *New Journal of Physics*, Vol. 19. ISSN 13672630. doi:10.1088/1367-2630/aa56a2.

Petyt, M., 2010. *Introduction to Finite Element Vibration Analysis*. Cambridge University Press, 2nd edition. doi: 10.1017/CBO9780511761195.

Thomes, R.L., Beli, D. and Marqui, C.D., 2022. "Space–time wave localization in electromechanical metamaterial beams with programmable defects". *Mechanical Systems and Signal Processing*, Vol. 167. ISSN 10961216. doi: 10.1016/j.ymssp.2021.108550.

Yang, Z., Gao, F., Shi, X., Lin, X., Gao, Z., Chong, Y. and Zhang, B., 2015. "Topological acoustics". *Phys. Rev. Lett.*, Vol. 114, p. 114301. doi:10.1103/PhysRevLett.114.114301. URL `https://link.aps.org/doi/10.1103/PhysRevLett.114.114301`.

Yin, J., Ruzzene, M., Wen, J., Yu, D., Cai, L. and Yue, L., 2018. "Band transition and topological interface modes in 1d elastic phononic crystals". *Scientific Reports*, Vol. 8. ISSN 20452322. doi:10.1038/s41598-018-24952-5.

Zak, 1989. "Berry's phase for energy bands in solids".

Zhao, D., Xiao, M., Ling, C.W., Chan, C.T. and Fung, K.H., 2018. "Topological interface modes in local resonant acoustic systems". *Physical Review B*, Vol. 98. ISSN 24699969. doi:10.1103/PhysRevB.98.014110.

Zhu, W., Ding, Y.Q., Ren, J., Sun, Y., Li, Y., Jiang, H. and Chen, H., 2018. "Zak phase and band inversion in dimerized one-dimensional locally resonant metamaterials". *Physical Review B*, Vol. 97. ISSN 24699969. doi: 10.1103/PhysRevB.97.195307.

7. ACKNOWLEDGEMENTS

The authors gratefully acknowledge the support of the Brazilian National Council for Scientific and Technological Development (CNPq) through Grant 308690/2019-2. The authors acknowledge the support of the Coordination of Superior Level Staff Improvement (CAPES) grant 88887.817136/2023-00. The authors also acknowledge the support of the Sao Paulo Research Foundation (FAPESP) grant 2018/15894-0 (thematic research project "Periodic structure design and optimization for enhanced vibroacoustic performance: ENVIBRO").